SCH13钢表面激光熔覆 CoNiCrAlY合金

张 松[1], 王明生[1], 张开祥[1], 张春华[1], 颜永根[2]
(1. 沈阳工业大学 材料科学与工程学院, 沈阳 110023; 2. 宝山钢铁股份有限公司研究院, 上海 201900)

张 松

摘 要: 采用 2 kW CO_2激光器在 SCH13钢表面激光熔覆 CoNiCrAlY合金, 选择最佳的工艺参数进行激光熔覆处理, 可获得性能优良的熔覆层组织. 利用扫描电子显微镜及能谱仪、X射线衍射仪、显微硬度计、磨损试验机对激光熔覆层的微观组织形貌、结构及成分、显微硬度和磨损性能进行了系统分析研究. 结果表明, CoNiCrAlY合金激光熔覆层与 SCH13钢基体存在良好的冶金结合, 熔覆层组织细密, 无裂纹, 稀释率较低, 界面处成分均匀平滑过渡; 熔覆层主要由 γ-Co, $FeCr_{0.29}Ni_{0.16}C_{0.05}$, FeNi, CoC_x及 $Cr_{23}C_6$组成; 熔覆层平均显微硬度较基体提高 3倍以上, 其相对耐磨性较基体提高了 3.42倍.

关键词: SCH13钢; 激光熔覆; CoNiCrAlY合金; 组织; 性能
中图分类号: TG174 文献标识码: A 文章编号: 0253-360X(2010)05-0049-04

0 序 言

SCH13钢高温强度高, 抗氧化性能好, 常用于高温炉底辊的生产. 目前冶金行业的高温炉辊表面大多采用爆炸喷涂高温抗氧化耐磨涂层的方法提高其表面性能, 但由于涂层与基体结合薄弱, 实际生产过程中炉辊表面涂层常有异常剥落现象发生, 从而给企业带来严重损失[1]. 激光表面改性是改善材料表面性能的有效方法[2,3], 钴基合金具有良好的耐高温性能和较好的耐磨性能, 因而经常作为激光熔覆材料, 但单一钴基合金熔覆层在高应力磨损时的耐磨性及抗热震性等有待于进一步提高. 目前, 含有稀土元素的钴基合金复合熔覆层的研究已成为新的研究热点, 研究表明, 在钴基合金中添加 Y, Y_2O_3等稀土元素及稀土氧化物可以明显提高复合熔覆层的高温和耐磨性能[4-6]. 作者旨在选用自行研制的 CoNiCrAlY合金粉末, 在冶金行业高温炉辊常用材料 SCH13钢表面进行激光熔覆处理, 对其组织结构及其性能进行系统研究, 为冶金行业高温炉辊的激光再制造提供理论依据.

1 试验方法

基体材料为 SCH13钢, 其化学成分 (质量分数, %) 为: Ni 12, Cr 26, C 0.35, 余量为 Fe; 样品尺寸为 60 mm×10 mm×5 mm; 激光熔覆用合金粉末为自行研制工业纯度的 CoNiCrAlY合金粉末, 平均粒度为 43~104 μm.

SCH13钢基材样品表面经 600号 SiC金相砂纸打磨、喷砂及清洗干燥后, 用粘结剂将 CoNiCrAlY合金粉末调制成糊状, 均匀地涂于待处理样品表面, 预置合金粉末层厚度为 0.5~0.7 mm, 自然晾干后, 经 120 ℃, 2 h烘干. 采用 2 kW CO_2激光加工成套设备进行激光熔覆处理, 优化工艺参数为: 输出功率 1 200 W, 光斑直径 φ2.5 mm, 扫描速度 10 mm/s, 大面积扫描搭接率为 50%. 依据生产实际情况, 熔覆过程中无气体保护.

取垂直于激光束扫描方向的横截面镶嵌后磨制成金相样品, 用 30 mL HCl+10 mL HNO_3腐蚀剂腐刻样品表面, 采用 BX60型系统显微镜和 IAS图象分析系统及 S-3400N型扫描电镜及其能谱仪分析激光熔覆层显微组织形貌和微区成分. 用 Philips PW3710 X射线衍射仪测定熔覆层的相结构, 其衍射条件为 CuKα衍射, 衍射束镍滤光器单色化, 电压为 40 kV, 电流为 35 mA, 扫描速度为 1.5°/min, 扫描范围为 20°~100°. 采用 HVS-1000数显显微硬度计测量熔覆层截面的显微硬度分布, 载荷为 19.6 N, 加载时间为 15 s; 采用 T-11球盘式磨损试验机进行磨损试验研究, 图 1为磨损试验机工作原理图. 磨损试验条件: 载荷为 30 N, 运动距离为 540 m, 机油润滑, 23 ℃室温条件, 测试试样为 SCH13钢基材

收稿日期: 2009-09-09
基金项目: 辽宁省教育厅研究发展计划资助项目(20060636); 沈阳市科技局攻关项目(108149-2-00, 1091242-6-00)

及激光熔覆样品，磨损样品尺寸为 ϕ25.6 mm×6 mm，样品表面粗糙度为 R_a=0.065 μm. 上试样为 ϕ6.35 mm的 Si_3N_4陶瓷球，粗糙度为 R_a=0.012 μm. 磨损后用 10倍低倍显微镜观察 Si_3N_4陶瓷球的表面形貌，未发现磨斑，可以将磨痕宽度转化为磨损体积 (ΔV)，即

$$\Delta V=2\pi r\left(R^2\arcsin(d/2R)-\frac{1}{2}d\sqrt{R^2-\frac{1}{4}d^2}\right)$$

式中：R为 Si_3N_4陶瓷球的半径；d为磨痕宽度；r为磨损半径. 熔覆层相对耐磨性表示为

$$\text{相对耐磨性}=\frac{\text{SCH13钢基材磨损体积}}{\text{激光溶覆层磨损体积}}$$

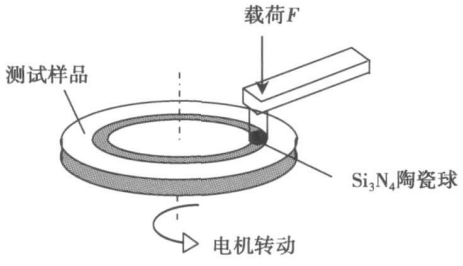

图 1 T-11磨损试验机工作原理简图

Fig. 1 T-11 wear test machine working principle gram

2 试验结果与分析

2.1 CoNiCrAlY合金激光熔覆层组织形貌

CoNiCrAlY合金粉末在激光束辐照过程中，位于熔池的不同位置其凝固条件不同，最终形成的显微组织形态不同[7].

图 2为激光熔覆层宏观组织形貌. 可以看出，熔覆层与基体相接处有一明显的白亮结合带，两者呈冶金结合. 白亮带的出现是由于激光熔覆加热和冷却速度极快，熔覆层与基材界面处温度梯度最大，在这种条件下，结晶潜热只能通过固相散出，相界面的推移受固相 (基体) 传热速度所控制[8,9]. 此时温度梯度是正值，当界面上个别凸起部分伸入温度较高的溶体中时，它的生长速度就会减慢甚至停止，周围部分的过冷度较凸起部分大，生长速度将增加，使凸起部分的生长优势消失，这种快速凝固过程使得液—固界面保持稳定的平面状态. 由单道次激光扫描熔覆层外观高宽比计算可知，激光热作用对基体的稀释率较低，在稀释率较低的情况下，采用光学显微镜即可观察到一条很窄的白亮结合带.

图 3为激光熔覆层各区域组织形貌. 溶覆层与

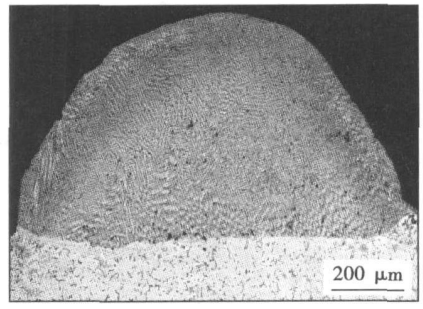

图 2 激光熔覆层宏观形貌

Fig. 2 OM micrograph of laser cladding layer

基体的结合处组织形貌呈现为垂直于界面方向生长的树枝晶 (图 3a所示)，枝晶的初生相为 γ-Co，枝晶间为共晶. 该区域一次枝晶很发达，二次枝晶欠发达，且部分一次枝晶干上不出现二次枝晶臂. 金属结晶在熔池中是择优生长的，即沿着温度梯度方向，以最快生长速度沿晶轴方向长大. 界面处熔池结晶时，由于基体蓄热量大，热量主要通过基体传导，熔池的底部与基体的冷金属接触，这样该处的结晶方向为传热的反方向，即与界面垂直. 图 3b为熔覆层中部组织形貌，该处熔池内熔体的散热条件变得越来越复杂，导致该处枝晶生长方向紊乱，而且随着液固界面的不断推进，液相中温度梯度不断降低，结晶速度加快，造成树枝晶呈逐渐细化趋势. 图 3c为熔覆层内组织形态发生转变区域的组织形貌，该区域组织呈现为树枝晶向等轴晶转变. 图 3d为熔覆层近表层组织，该处为平行于激光扫描方向细密的等轴晶生长区，由于熔覆层表面的温度较高，基体对熔池表面散热的影响有限，已凝固的熔覆层成为熔池

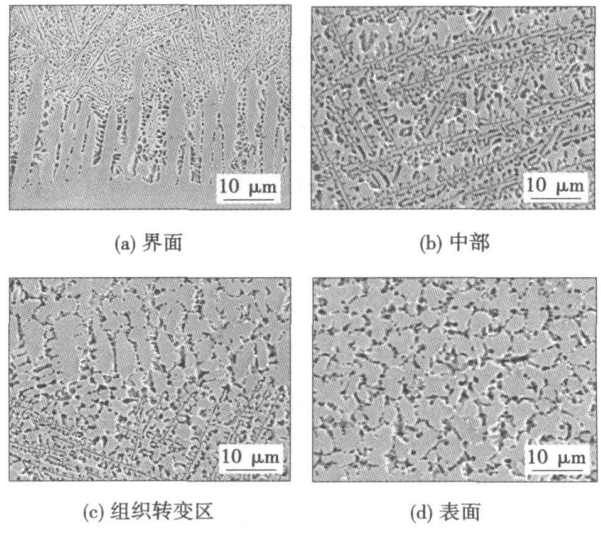

图 3 激光熔覆层各区域组织形貌

Fig. 3 SEM micrographs of laser cladding layer

热传导的主要通道，温度梯度降低，故表面形成平行于激光束扫描方向的等轴晶.

2.2　CoNiCrAlY合金激光熔覆层相组成

图 4为 CoNiCrAlY合金激光熔覆层 X射线衍射谱. 分析可知，激光熔覆层主要由 γ-Co，$FeCr_{0.29}Ni_{0.16}C_{0.06}$，FeNi，$CoC_x$和 $Cr_{23}C_6$等相组成. γ-Co仅在 417 ℃以上稳定存在，室温下钴基固溶体为六方点阵. 高温下的 γ-Co由于快速凝固以及随后的快速冷却，来不及发生相变，故熔覆层中钴基固溶体为面心立方结构的 γ-Co亚稳相，此外镍有稳定面心立方结构钴基固溶体的作用. 硬质碳化物及金属间化合物将对提高熔覆层的性能起到有益作用.

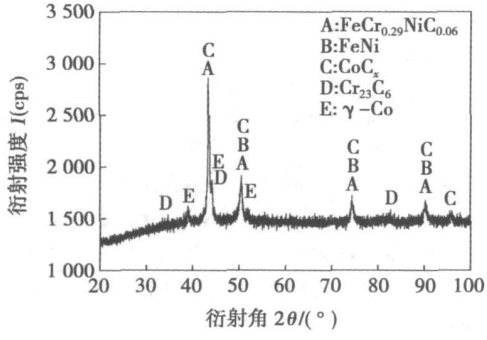

图 4　激光熔覆层 X射线衍射谱

Fig. 4　XRD spectrum of laser cladding specimen

图 5为激光熔覆层局部区域组织形貌，对图 5中一次枝晶干（A区域）及颗粒相（B点）进行 EDS分析，其结果如表 1所示. 由表 1分析结果可知，Ni，Co，Fe，Al，Si等元素主要固溶于初生相 γ-Co中，故 γ-Co为溶有多种元素的钴基固溶体. B点所示的颗粒相为富含 Al，Y元素的合金化合物，由于其量少，且细小弥散，在 X射线衍射相分析中难以检测出来.

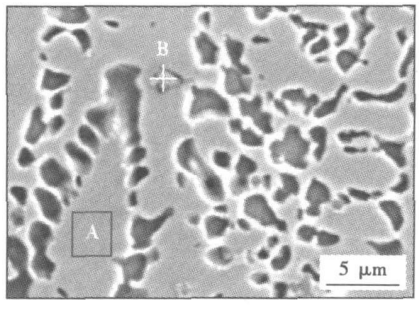

图 5　激光熔覆层局部区域组织形貌

Fig. 5　Local regional microstructure of laser cladding layer

表 1　激光熔覆层 EDS分析结果（质量分数，%）

Table 1　EDS analysis results of laser cladding specime

位置	Co	Ni	Cr	Fe	Al	Si	Y
A区	33.3	28.4	22.4	7.6	7.6	0.6	—
B点	23.0	19.0	19.3	4.7	22.3	0.7	11.0

2.3　CoNiCrAlY合金激光熔覆层的耐磨性

图 6为 CoNiCrAlY合金激光熔覆层显微硬度分布曲线. 可以看出，硬度分布曲线呈现三个台阶，它们分别对应于基体、热影响区和熔覆层区域，因为热影响区区域较小，对应热影响区的台阶不是很明显. 热影响区的显微硬度为 250 HV左右，这较基体的显微硬度 200 HV略高，这是由于在激光熔覆过程中，靠近熔覆层的基体组织发生奥氏体化，碳化物溶解或部分溶解，且加热时间较短和冷却速度极快，碳来不及进行均匀扩散而形成淬硬组织细小的高碳马氏体和少量的残余奥氏体，因此造成了该区域的硬化现象. CoNiCrAlY合金熔覆层的硬度在 600～750 HV之间，熔覆层的硬度得到了较大幅度的提高，是因为熔覆合金粉末中有大量的合金元素，激光熔覆为快速凝固过程，其过饱和固溶体的固溶强化作用显著，同时快速熔凝及稀土元素 Y的加入，使得合金熔覆层晶粒得到明显细化. 由熔覆层硬度分布曲线可以看出，熔覆层表层硬度较次表层略有下降，这是因为在激光熔覆过程中熔池内的对流传质作用能充分搅拌熔池，使熔池中的气体、夹杂物和一些非金属元素上浮析出，从而在熔覆层表层形成相对疏松的组织，同时高的表层温度可导致熔池表层部分合金元素烧损所致. 熔覆层中部因拥有细密的组织而具有最高硬度，随着熔深的增加，组织粗化及基体元素向熔覆层的熔入，硬度缓慢下降，并在界面处发生突变.

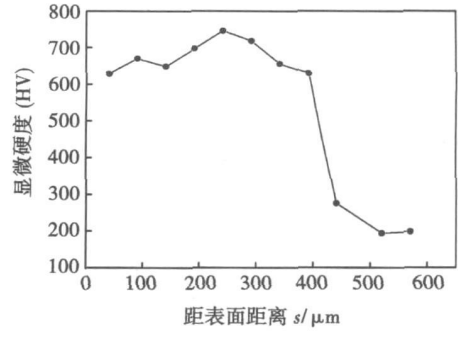

图 6　激光熔覆层截面硬度分布曲线

Fig. 6　Hardness profile along melt depth of laser cladding specimen

表 2为 CoNiCrAlY合金激光熔覆层及 SCH13

钢基材磨损试验结果,可以看出,SCH13熔覆 CoNiCrAlY合金后其相对耐磨性得到了大幅度的提高,约为基体的 4.42倍.

表 2 激光熔覆及基材样品磨损试验结果

Table 2 Wear resistance comparison between SCH13 steel and coating

材料	磨痕宽度平均值 D/mm	磨损体积 V/mm³	相对耐磨性 ε
激光熔覆层	1.16	2.599	4.42
SCH13钢	1.89	11.494	—

3 结 论

(1)选择合理的激光熔覆工艺参数,可在 SCH13钢表面获得稀释率低、无裂纹、与基体达到良好冶金结合的 CoNiCrAlY合金熔覆层,熔覆层组织细密.

(2)CoNiCrAlY合金激光熔覆层主要由 γ-Co,$FeCr_{0.29}Ni_{0.16}C_{0.06}$,FeNi,$CoC_x$和 Cr_7C_3等相组成,熔覆层中存在富含稀土 Y及 Al元素的微量合金化合物颗粒相.

(3)激光熔覆层的硬度较 SCH13钢基体有了很大的提高,平均硬度在 600 HV以上,CoNiCrAlY合金熔覆层相对耐磨性较基体提高了 3.42倍.

参考文献:

[1] Yuan F H, Chen Z X, Huang Z W, et al. Oxidation behavior of thermal barrier coatings with HVOF and detonation-sprayed NiCrAlY bond coats[J]. Corrosion Science, 2008, 50(6): 1608—1617.

[2] 张春华, 张 宁, 张 松, 等. 6061铝合金表面激光熔覆温度场的仿真模拟[J]. 沈阳工业大学学报, 2007, 29(3): 266—270.
Zhang Chunhua, Zhang Ning, Zhang Song, et al. Simulation and experimental investigations of laser cladding temperature field on 6061 Al alloy[J]. Journal of Shenyang University of Technology, 2007, 29(3): 266—270.

[3] 张 松, 胡金玲, 王 强, 等. 医用钛表面激光显微加工工艺参数的优化[J]. 沈阳工业大学学报, 2008, 30(4): 424—428.
Zhang Song, Hu Jinling, Wang Qiang, et al. Parameters optimization of laser micromachining of biomedical titanium[J]. Journal of Shenyang University of Technology, 2008, 30(4): 424—428.

[4] 杨尚磊, 张文红, 李法兵, 等. 纳米 Y_2O_3-Co基合金激光熔覆复合涂层的分析[J]. 焊接学报, 2009, 30(2): 79—82.
Yang Shanglei, Zhang Wenhong, Li Fabing, et al. Investigation on laser cladded nano-Y_2O_3 and cobalt based composite coating[J]. Transactions of the China Welding Institution, 2009, 30(2): 79—82.

[5] Zhang Shihong, Li Mingxi, Jae Hong Yoon, et al. Effect of the addition of Sm_2O_3 on the microstructure of laser cladding alloy coating layers[J]. Metals and Materials International, 2008, 14(3): 315—319.

[6] Wang Xinhong, Zou Zengda, Qu Shiyao, et al. Modifying effect of rare earth La_2O_3 on the Fe-C-Cr-Si-B laser clad coatings[J]. Journal of Materials Science Letters, 2003, 22(10): 713—715.

[7] 张 松, 张春华, 李春燕. 热作模具钢表面激光熔覆 Stellite X-40钴基合金[J]. 焊接学报, 2005, 26(1): 17—20.
Zhang Song, Zhang Chunhua, Li Chunyan. Laser cladding Stellite X-40 Co-based alloy on hot die steel[J]. Transactions of the China Welding Institution, 2005, 26(1): 17—20.

[8] Hunt J D. Pattern formation in solidification[J]. Science and Technology of Advanced, 2001, 2(1): 147—155.

[9] Toyserkani E, Khajepour A, Corbin S. Laser cladding[M]. Boca Raton: CRC Press, 2005.

作者简介:张 松,女,1963年出生,博士,教授.研究方向为材料表面改性及激光先进制造技术.发表论文 90余篇.

Email: songzhang_sy@yahoo.com.cn

proach for the sub-system of plasma jet generation was presented in this paper based on the rule sets supervision and multi-model adaptive control system structure.

Key words: plasma spraying; plasma jet morphology; intelligent control; data mining; clustering analysis

Brazing of aluminum matrix composites SiC_p/ZL101 to Kovar alloy 4J29 NIU Jitai[1,2], LU Jinbin[1], MU Yunchao[1], LUO Xiangwei[3] (1. Department of Materials and Chemical Engineering, Zhongyuan University of Technology, Zhengzhou 450007, China; 2. State Key Laboratory of Advanced Welding Production Technology, Harbin Institute of Technology, Harbin 150001, China; 3. Department of Materials Science & Engineering, Zhengzhou University, Zhengzhou 450002, China). p 37 - 40

Abstract: SiC_p/ZL101 composites containing 55% SiC_p and Kovar alloy 4J29 were chosen as base metals. After being electroplated by Ni on the SiC_p/ZL101, the two materials were brazed by Zn-Cd-Ag as filler metal at the 420 ℃ for 7 min. Moreover, the interfacial microstructures and fracture appearances were investigated by SEM and EDS. The results show that the electroplated Ni on the surface of SiC_p/ZL101 can improve the filler's wettability to the composite material. There are transition layers not only between the filler and Kovar alloy, but also between the filler and the electroplated Ni layer, which shows the filler metal, the electroplated Ni layer, the composites and Kovar alloy can realize metallurgically joining by diffusion. The fracture analysis shows that the fracture happens inside the composites near the electroplated Ni layer.

Key words: aluminum matrix composites; Kovar alloy; brazing Ni electroplating

Analysis of chemical reaction on weld pool surface in activating TIG welding of aluminum alloys HUANG Yong, FAN Ding, SHAO Feng (State Key Laboratory of New Non-ferrous Metal Materials, Lanzhou University of Technology, Lanzhou 730050, China). p 41 - 44

Abstract: For activating TIG welding of aluminum alloys, including A-TIG welding, FB-TIG welding and FZ-TIG welding, the analysis of chemical reaction between the activating fluxes and the weld pool metal has great significance to certain the feasibility of these welding processes and instruct the developments of activating fluxes. Through the XRD analysis of weld surface slag, the chemical reaction thermodynamics was calculated based on functional determinant of Gibbs' Free Energy, and the chemical reaction on welding pool was analyzed. It is found that, for the FZ-TIG welding, with multi-component flux FZ108 developed by authors as central region flux and SiO_2 as outer region flux, the endothermic reactions between flux FZ108 and the welding pool metal can constrict the arc and increase weld penetration. For the A-TIG welding with flux FZ108, the few absorbed heat or the released heat of the chemical reactions has small influence on the arc. For the FB-TIG welding with flux SiO_2, the chemical reaction between the flux and the weld pool metal and its surface oxide film does not happen, and the arc is not affected through these chemical reactions.

Key words: aluminum alloy; A-TIG welding; activating flux; chemical reaction; arc constriction

Microstructures and mechanical properties of transient liquid phase bonded Ti_3Al based alloy joints GU Xiaoyan[1], SUN Daqian[1], REN Zhen'an[1], LIU Li[2], DUAN Zhenzhen[2] (1. Key Laboratory of Automobile Materials, Jilin University, Changchun 130025, China; 2. Changchun Railway Vehicles Co., LTD., Changchun 130062, China). p 45 - 48

Abstract: Microstructure and mechanical properties of Ti_3Al based alloy joints bonded by transient liquid phase bonding were studied by scanning electron microscope (SEM), energy dispersive X-ray spectroscope (EDS), X-ray diffraction (XRD) and universal test machine. The results show that the integrated joints were prepared by TLP bonding with the TiZrNiCu alloy interlayer. The high bonding temperature and long bonding time help to obtain the joints with uniform composition and microstructure. With bonding temperature and bonding time increasing, the width of the bonding zone increases and reaction zones decreases. When bonding time is 60 min at bonding temperature of 900 ℃, the joint microstructure consists of Ti solid solution, Ti_3Al and Ti_2Cu and the joint strength of 420 MPa can be obtained.

Key words: Ti_3Al based alloy; transient liquid phase diffusion bonding; microstructure; shear strength

CoNiCrAlY alloy deposited on surface of SCH13 steel by laser cladding ZHANG Song[1], WANG Mingsheng[1], ZHANG Kaixiang[1], ZHANG Chunhua[1], YAN Yonggen[2] (1. School of Materials Science and Engineering, Shenyang University of Technology, Shenyang 110023, China; 2. Baoshan Iron & Steel Co., Ltd., Shanghai 201900, China). p 49 - 52

Abstract: The surface of SCH113 steel was deposited with CoNiCrAlY alloy by a high power CO_2 laser. Through, the excellent coatings can be acquired by the optimized process parameters. The micro-structure, composition, hardness and corrosive resistance of the coating were examined by scanning electron microscope (including EDS microanalysis), X-ray diffraetometry, micro thickness meter, wear test machine. The results indicated that the coating of CoNiCrAlY alloy has a good metallurgical combination with SCH13 steel, and the other characteristics such as fine microstructure, no cracks, low dilution rate and the smooth transition of elements at the interface. The coatings were consisted of γ-Co, $FeCr_{0.29}Ni_{0.16}C_{0.06}$, FeNi, CoC_x and $Cr_{23}C_6$ phases. The average microhardness of the coating is 3 times higher than that of the SCH13 steel. Furthermore, the wear resistance of laser cladded coating is 3.42 times higher than that of the matrix.

Key words: SCH13 steel; laser cladding; CoNiCrAlY alloy coatings; microstructure; property

Electron beam welding of TA15 titanium alloy to 304 stainless steel WANG Ting, ZHANG Binggang, CHEN Guoqing, FENG Jicai (State Key Laboratory of Advanced Welding Production Technology, Harbin Institute of Technology, Harbin 150001, China). p 53 - 56

Abstract: Electron beam welding experiment of TA15 titanium alloy to 304 stainless steel was carried out. Microstructure and micro-hardness distribution of joint were examined. The results showed that the weldability of electron beam welding of TA15 titanium alloy to 304 stainless steel was so poor that many